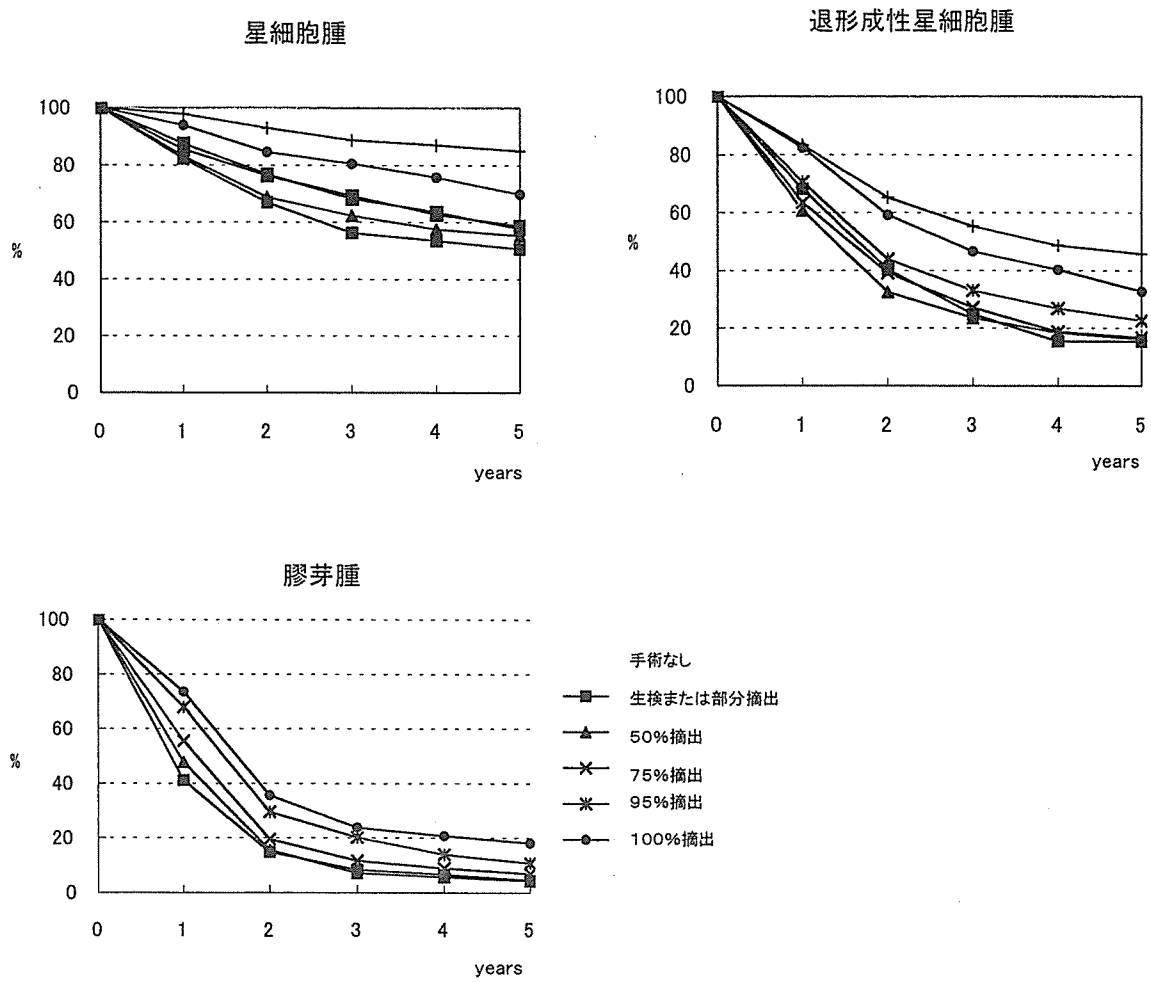

図５　手術摘出度によるグリオーマの生存率

おわりに

脳腫瘍の標準的治療を確立していくためには，確実なデータ管理のもとで，最もエビデンスレベルの高いランダム化臨床試験を行っていく必要がある．これに対し，疫学や統計は，過去の臨床例のデータの解析から，その疾患の特性を知り，有効な治療法を見つけ出そうというものである．ある環境条件が腫瘍の発生に影響をもつという事実を証明するには，大規模な調査が必要となるが，そこから得られた結果は予防医学へ通じるものであり，きわめて重要な情報を我々に提供してくれると考えられる．

参考文献

1. Kleihues P, Ohgaki H (1999) Primary and secondary glioblastomas: from concept to clinical diagnosis. Neuro-Oncol 1: 44-51
2. Malmer B, Iselius L, Holmberg E, Collins A, Henriksson R, Gronberg H (2001) Genentic epidemiology of glioma. Br J Cancer 84: 429-434
3. Grossman SA, Osman M, Hruban R, Piantadosi S (1999) Central nervous system cancers in the first-degree relatives and spouses. Cancer Invest 17: 299-308
4. Hu J, Mao Y, Ugnat AM (2000) Parental cigarette smoking, hard liquor consumption and the risk of childhood brain tumors- a case control study in northeast China. Acta Oncol 39: 979-984
5. Thomas TL, Stolley PD, Stemhagen A, Fontham ET, Bleecker ML, Stewart PA, Hoover RN (1987) Brain tumor mortality risk among men with electrical and electronics jobs: a case-control study. J Natl Cancer Inst 79: 233-238
6. Bohnen NI, Kurland LT (1995) Brain tumor and exposure to pesticides in humans: a review of the epidemiologic data. J Neurol Sci 132: 110-121
7. Preston-Martin S, Mack W, Henderson BE (1989) Risk factors for gliomas and meninigiomas in males in Los Angels County. Cancer Res 49: 6137-6143
8. Karlsson P, Holmberg E, Lundell M, Mattsson A, Holm LE, Wallgren A (1998) Intracranial tumors after exposure to ionizing radiation during infancy: a period analysis of two Swedish cohorts of 28,008 infants with skin hemangioma. Radiat Res 150: 357-364
9. Shapiro S, Mealey J Jr, Sartorius C (1989) Radiation-induced intracranial malignant gliomas. J Neurosurg 71: 77-82
10. Salvati M, Artico M, Caruso R, Rocchi G, Orlando ER, Nucci F, Salvati M (1991) A report on radiation-induced gliomas. Cancer 67: 392-397
11. Muscat JE, Malkin MG, Thompson S, Shore RE, Stellman SD, McRee D, Neugut AI, Wynder EL (2000) Handheld cellular telephone use and risk of brain cancer. JAMA 284: 3001-3007
12. Central brain tumor registry of the United States: CBRUS (2004). Statistical report: primary brain tumors in the United States, 1997-2001
13. Jukich PJ, McCarthy BJ, Surawicz TS, Freels S, Davis FG (2001) Trends in incidence of primary brain tumors in the United States, 1985-1994. Neuro-Oncol 3: 141-151
14. Legler JM, Ries LA, Smith MA, Warren JL, Heineman EF, Kaplan RS, Linet MS (1999) Brain and other central nervous system cancers: recent trends in incidence and mortality. J Natl Cancer Inst 91: 1382-1390
15. The Committee of Brain Tumor Registry of Japan (2003) Report of brain tumor registry of Japan (1969-1996) 11th edition. Neurol med-chirur 43 (suppl)
16. Winger MJ, Macdonald DR, Cairncross JG (1989) Supratentorial anaplastic gliomas in adults: the prognositic importance of extent of resection and prior low-grade glioma. J Neurosurg 71: 487-493
17. Anderson AP (1978) Postoperative irradiation of glioblastoma. Acta radiol 17: 475-484
18. Walker MD, Green SB, Byar DP, Alexander E Jr, Batzdorf U, Brooks WH, Hunt WE, MacCarty CS, Mahaley MS Jr, Mealey J Jr, Owens G, Ransohoff J 2nd, Robertson JT, Shapiro WR, Smith KR Jr, Wilson CB, Strike TA (1980) Randomized comparisons of radiotherapy and nitrosoureas for the treatment of malignant glioma after surgery. N Eng J Med 303: 1323-1329
19. Chang CH, Horton J, Schoenfeld D, Salazer O, Perez-Tamayo R, Kramer S, Weinstein A, Nelson JS, Tsukada Y (1983) Comparison of postoperative radiotherapy and combined postoperative radiotherapy and chemotherapy in the multidisciplinary management of malignant gliomas. Cancer 52: 997-1007
20. Stewart LA, Glioma Meta-analysis Trialists (GMT) (2002) Chemotherapy in adult high-grade glioma:

a systematic review and meta-analysis of individual patient data from 12 randomised trials. Lancet 359: 1011-1018

21. Hensley ML, Schuchter LM, Lindley C, Meropol NJ, Cohen GI, Broder G, Gradishar WJ, Green DM, Langdon RJ Jr, Mitchell RB, Negrin R, Szatrowski TP, Thigpen JT, Von Hoff D, Wasserman TH, Winer EP, Pfister DG (1999) American Society of Clinical Oncology clinical practice guidelines for the use of chemotherapy and radiotherapy protectants. J Clin Oncol 17: 3333-3355

Acta Neurochir (Wien) (2006)
DOI 10.1007/s00701-006-0857-7

Acta Neurochirurgica
Printed in Austria

Clinical Article

Surgical resection of tumors located in subcortex of language area

K. Sakurada, S. Sato, Y. Sonoda, Y. Kokubo, S. Saito, and **T. Kayama**

Department of Neurosurgery, Yamagata University, School of Medicine, Yamagata, Japan

Received December 6, 2004; accepted July 26, 2006; published online September 29, 2006

Summary

Object. Although functional mapping facilitates the planning of surgery in and around eloquent areas, the resection of tumors adjacent to language areas remains challenging. In this report, we took notice that the language areas (Broca's and Wernicke's) present at the perisylvian fissure. We posit that if there is non-essential language area on the inner surface of the Sylvian fissure, safe tumor resection may be possible even if the tumor is located under the language cortex.

Methods. The study population consisted of 5 patients with intrinsic brain tumors (frontal glioma, $n = 3$; temporal cavernous angioma, $n = 1$; primary malignant central nervous system lymphoma, $n = 1$) located in the perisylvian subcortex, in the language-dominant hemisphere. All patients underwent awake surgery and we performed intra-operative bipolar cortical functional language mapping. When the tumor was located under the language area, the Sylvian fissure was opened and the inner surface of the opercular cortex was exposed with the patient asleep, and additional functional mapping of that cortex was performed. This enabled us to remove the tumor from the non-functioning cortex.

In our series, 4 of 5 patients had not language function on the inner surface of the operculum. Only one patient, a 52-year-old man with frontal glioblastoma (Case 3) had language function on the inner surface of the frontal operculum.

Conclusion. We suggest that even perisylvian tumors located in the subcortex of the language area may be resectable via the nonfunctioning intrasylvian cortex by a transopercular approach without resultant language dysfunction.

Keywords: Functional mapping; language area; operculum; brain tumor.

Introduction

To minimize the risk of postoperative language deficits in patients scheduled for surgery near the perisylvian cortex in the dominant hemisphere, knowing the localization of language function is important for planning the cortical trajectory and the resection area. While reports on language cortical and subcortical mapping using awake craniotomy and/or a sub-dural grid are available [13, 14, 19], surgical resection under the eloquent cortices continues to present a high risk of neurological sequelae. Neuro-imaging functional techniques are in development and are beginning to be efficient for cortical sensorimotor mapping, but still lack sensitivity and specificity for language mapping, and remain difficult to give real-time data during surgery [16].

The supratemporal plane is divided into the three parts (planum polare, Heschl gyrus, planum temporale), and contains the primary and association auditory system and a part of Wernicke's area. However, the language function of the inner surface of the operculum, and the clinical presentation and treatment of patients with lesions in these areas have rarely been described.

Here we present the results of functional mapping and surgery undergone by 5 patients with tumors located in and around the subcortex of the language area. These lesions can be resected safely using functional mapping in patients undergoing awake surgery.

Methods

Subjects

There were 5 patients with intrinsic brain tumors (frontal glioma, $n = 3$; temporal cavernous angioma, $n = 1$; temporal primary central nervous system malignant lymphoma, $n = 1$) located in the perisylvian subcortex in the language-dominant hemisphere. They were 2 men and 3 women; their median age was 46 years (range 31–55 years) (Table 1a).

Language evaluation

The Standard Language Test of Aphasia (SLTA) was used to evaluate language functions. The SLTA is the standardized test battery most

Table 1a. *Summary of the 5 patients*

Case	Age (yr), sex	Diagnosis	Tumor localization	Handedness	Language dominancy	Initial symptom
1	49 F	malignant lymphoma	lt. temporal	Rt.	Lt.	epilepsy
2	31 F	astrocytoma	lt. frontal	Rt.	Lt.	inicidental
3	52 M	glioblastoma	lt. frontal	Rt.	Lt.	hemiparesis
4	55 M	oligodendroglioma	lt. frontal	Rt.	Lt.	epilepsy
5	44 F	cavernous angioma	lt. temporal	Rt.	Lt.	transient paraphasia

Table 1b. *Summary of the severity of aphasia in the 5 patients*

Case	Overall SLTA severity		Auditory comprehension		Naming		Sentence repetition		Sentence reading aloud		Reading comprehension		Kana letter dictation		Sentence dictation	
	pre	post	pre	post	pre	post	pre	post	pre	post	pre	post	pre	post	pre	post
1	10	10	7	9	16	18	3	5	4	5	7	9	10	8	5	5
2	10	10	10	10	20	20	5	4	5	5	10	10	10	10	5	5
3	5	9	1	1	14	14	3	4	5	5	1	1	6	8	1	1
4	10	10	9	8	18	18	4	4	5	5	10	10	10	10	5	5
5	10	10	10	10	20	20	4	4	5	5	8	8	10	10	5	5

commonly used to evaluate Japanese aphasic patients [20]. The aphasia severity ratings (0 = most severe, 10 = normal) are based on the 19 SLTA sub-scores; these were used as the primary language measure in the present study [8, 11]. The following seven subscores of the SLTA were also included in the analysis: auditory comprehension (to obey verbal commands) (out of 10); naming (out of 20); sentence repetition (out of 5); reading aloud short sentences (out of 10); dictation of Kana letters (out of 10); and dictation of short sentences (out of 5). Each patient was given the SLTA twice; the aphasia severity ratings before and after the operation (approximately 1 to 3 months after the surgery) are shown in Table 1b.

Intra-operative cortical functional mapping

To determine whether the lesions were located in the dominant hemisphere, patients underwent pre-operative functional MRI and/or intracarotid amytal testing (Wada test). During awake surgery, intra-operative cortical mapping for language was performed in all patients following the previous reports [1, 10, 14]. Intravenous anesthesia (propofol) was used during craniotomy. After creating a cranial opening large enough to expose most of the lateral temporal and inferior frontal lobe, propofol administration was discontinued and the patient was allowed to awaken. Silver-tip bipolar electrodes spaced approximately 5 mm from each other were placed on the exposed cortical surface. Stimulation parameters are set at 60 Hz, biphasic square wave pulses (1 msec/phase), with variable peak-to-peak current amplitude between 2 to 12 mA (peak-peak amplitude). To avoid eliciting local seizure phenomena or false negative or false positive results, a current below the after-discharge threshold was used so that depolarization was not propagated to the nearby cortex. Before mapping, 10 to 20 sites were selected and marked with small tags. Sites for stimulation mapping were randomly selected to cover all of the exposed frontal or temporal lobe cortex, including areas thought to contain sites essential for language function and areas near and overlying the lesion site. Each patient was shown images of simple objects. Cortical stimulation, applied before the presentation of each image, was continued until there was a correct response or the next image was presented. Each pre-selected site was stimulated 3 to 4 times but never twice in succession. Sites where stimulation produced consistent speech arrest or anomia were considered essential language areas.

Case illustration

Case 1

This 49-year-old right-handed woman was in excellent health when she had her first generalized tonoclonic seizure. Preoperative MRI showed a round well-enhanced 2.5 cm lesion in the superior temporal gyrus. Intra-operative functional mapping of the essential speech cortex under awake surgery disclosed that the tumor was located just under the temporal language area. After exposing the posterior part of superior temporal plane by

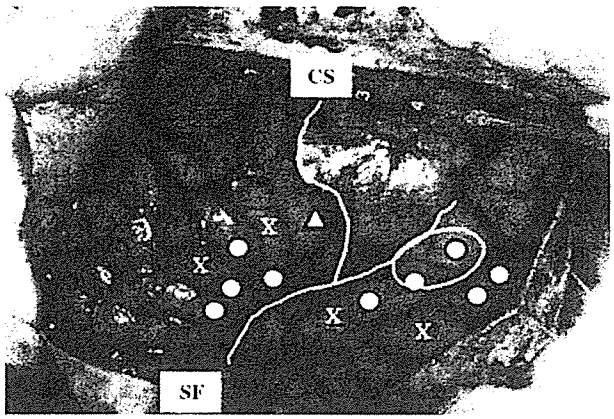

Fig. 1. *Case 1* – A 49-year-old woman with primary CNS malignant lymphoma. Intra-operative photograph of the brain map showing that the tumor is located under the Wernicke's area. ○ Speech arrest, △ dysarthria, × no response, *CS* central sulcus, *SF* Sylvian fissure

opening the Sylvian fissure, we performed intra-operative language mapping of the posterior part of the superior temporal plane. No language site was identified at that area. Unfortunately, we could not obtain an intra-operative pathological diagnosis, so we totally removed the lesion via a superior temporal plane cortical incision (Fig. 1). Postoperative histological diagnosis was primary CNS malignant lymphoma. This was treated with radio-chemotherapy as adjuvant therapy. Her postoperative SLTA score remained unchanged. She discharged from our hospital without any neurological deficits.

Case 2

This 31-year-old woman was in excellent health when she sustained a simple head injury. CT study incidentally disclosed an anomaly. Preoperative MRI revealed a round, non-enhancing, 3 cm lesion in the inferior frontal gyrus. With the patient awake, intra-operative cortical functional mapping of the essential speech cortex was performed. A frontal language area was identified; the tumor was located under the tongue motor area. We exposed the frontal operculum by opening the Sylvian fissure and performed intra-operative language mapping. No language function was identified at the inner surface of the posterior part of the frontal operculum; the tumor was removed from the non language area (Fig. 2). The histological diagnosis was low-grade astrocytoma. Although she suffered transient dysarthria, she fully recovered within several days.

Case 3

This 52-year-old right-handed man was admitted to our hospital with aphasia and right-hand loss of power to grip. MRI showed a ring-like enhanced lesion in the frontal lobe. Intra-operative cortical language mapping

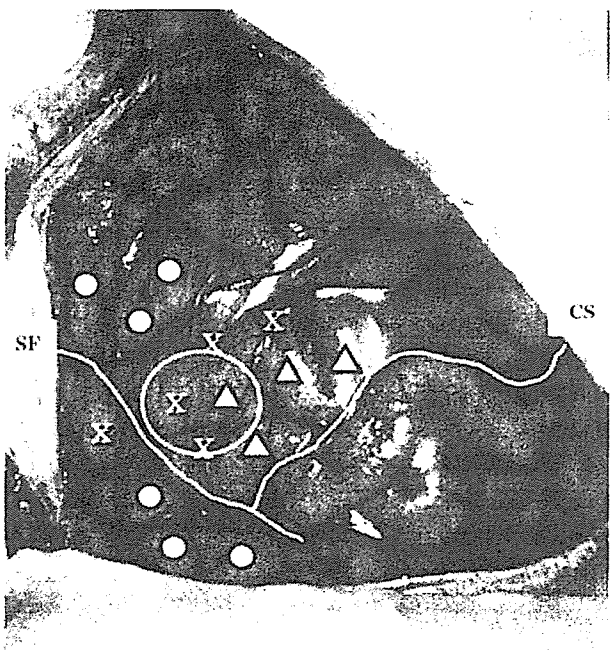

Fig. 2. *Case 2* – A 31-year-old woman with low-grade astrocytoma. Intra-operative photograph of the brain map showing that the tumor is located within the tongue motor area. ○ Speech arrest, △ dysarthria, × no response, *CS* central sulcus, *SF* Sylvian fissure

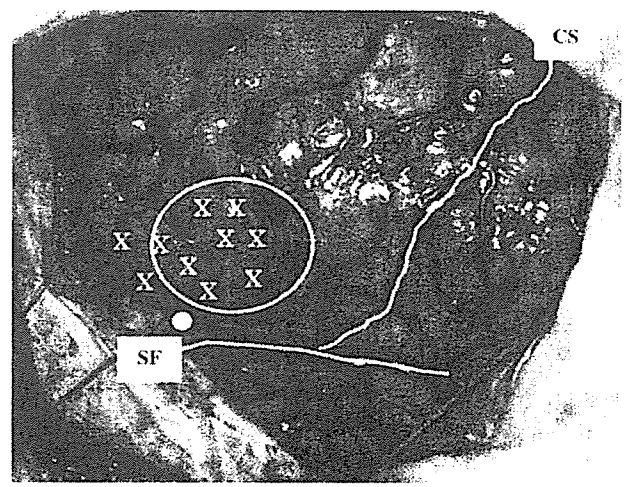

Fig. 3. *Case 3* – A 52-year-old man with frontal glioblastoma multiforme. Intra-operative photograph of the brain map showing that the Broca's area is located on the inside of the Sylvian fissure. ○ Speech arrest, △ dysarthria, × no response, *CS* central sulcus, *SF* Sylvian fissure

failed to identify a frontal language area. His inferior frontal gyrus was swollen. We exposed the inner surface of the frontal operculum by opening the Sylvian fissure and performed intra-operative language mapping again. The essential language area, located on the inner surface of the frontal operculum, was compressed by a tumor and shifted into the Sylvian fissure. We resected the tumor through the non-language cortex (Fig. 3). The language area was replaced to the surface of inferior frontal gyrus. The histological diagnosis was glioblastoma multiforme. His overall SLTA severity had worsened immediately after the operation, whereas it recovered and improved 3 months after surgery (Table 1b).

Case 4

This 55-year-old-man was admitted our hospital with transient epileptic motor aphasia. T1- and T2-weighed MRI showed a low- and a high-intensity lesion in the inferior frontal gyrus, respectively, which was not enhanced by gadolinium. His pre-operative interictal SLTA score was normal. During awake surgery, intra-operative functional mapping identified a frontal language area. The tumor was located under the language area. We opened the Sylvian fissure and performed intra-operative language mapping at the inside of the Sylvian fissure again. Because no essential language area was identified on the inner surface of the frontal operculum, we resected the tumor through this non-language area (Fig. 4). The histological diagnosis was oligodendroglioma. His postoperative SLTA score was also normal.

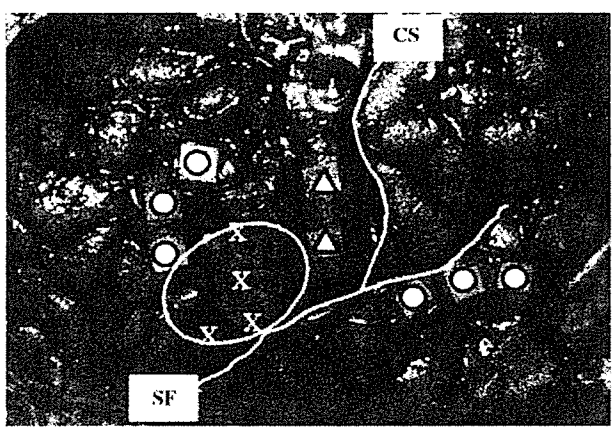

Fig. 4. *Case 4* – A 55-year-old man with oligodendroglioma. Intra-operative photograph of the brain map showing that the tumor is located under the Broca area. ○ Speech arrest, △ dysarthria, × no response, *CS* central sulcus, *SF* Sylvian fissure

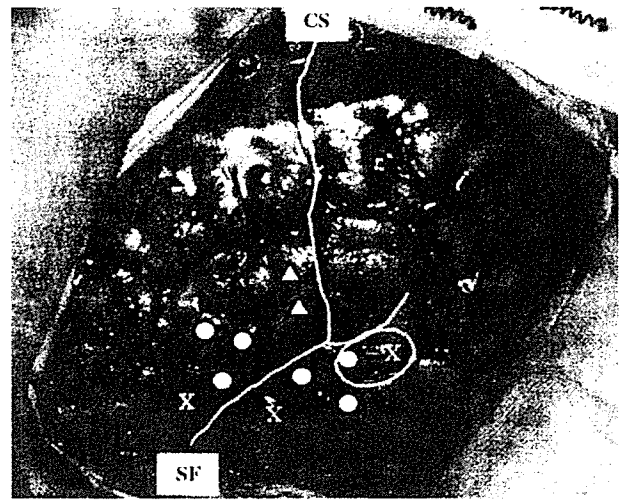

Fig. 5. *Case 5* – A 44-year-old woman with cavernous angioma. Intra-operative photograph of the brain map showing that the tumor is located under the Wernicke area. ○ Speech arrest, △ dysarthria, × no response, *CS* central sulcus, *SF* Sylvian fissure

Case 5

This 44-year-old woman visited our hospital complaining of transient paraphasia. T2-weighted MRI showed a mixed-intensity lesion with a hypo-intense rim in the left superior temporal gyrus. Awake craniotomy was performed. Intra-operative functional mapping revealed that the tumor was located under Wernicke's area. We opened the Sylvian fissure and performed intra-operative language mapping of the planum temporale. No language function was identified at that area. We resected the tumor through the non-language area on the splanum temporale (Fig. 5). The diagnosis was cavernous angioma. Her postoperative SLTA score was normal.

Summary of cases

Pre- and postoperative MRI of the 5 patients are shown in Fig. 6. Quality of resection was systemically evaluated using immediate (within 72 hr after the operation) post-operative MRI. We were able to remove all tumors totally without permanent new neurological deficits and without exacerbation of the patients' aphasia. Schematic drawings presented in Fig. 7 identify the localization of the 5 tumors and the language areas. Of the 5 patients, only case 3, a patient with frontal glioblastoma manifested essential language function on the inner surface of the frontal or temporal operculum. This language area, located on the frontal operculum, appeared to be compressed and displaced by the tumor.

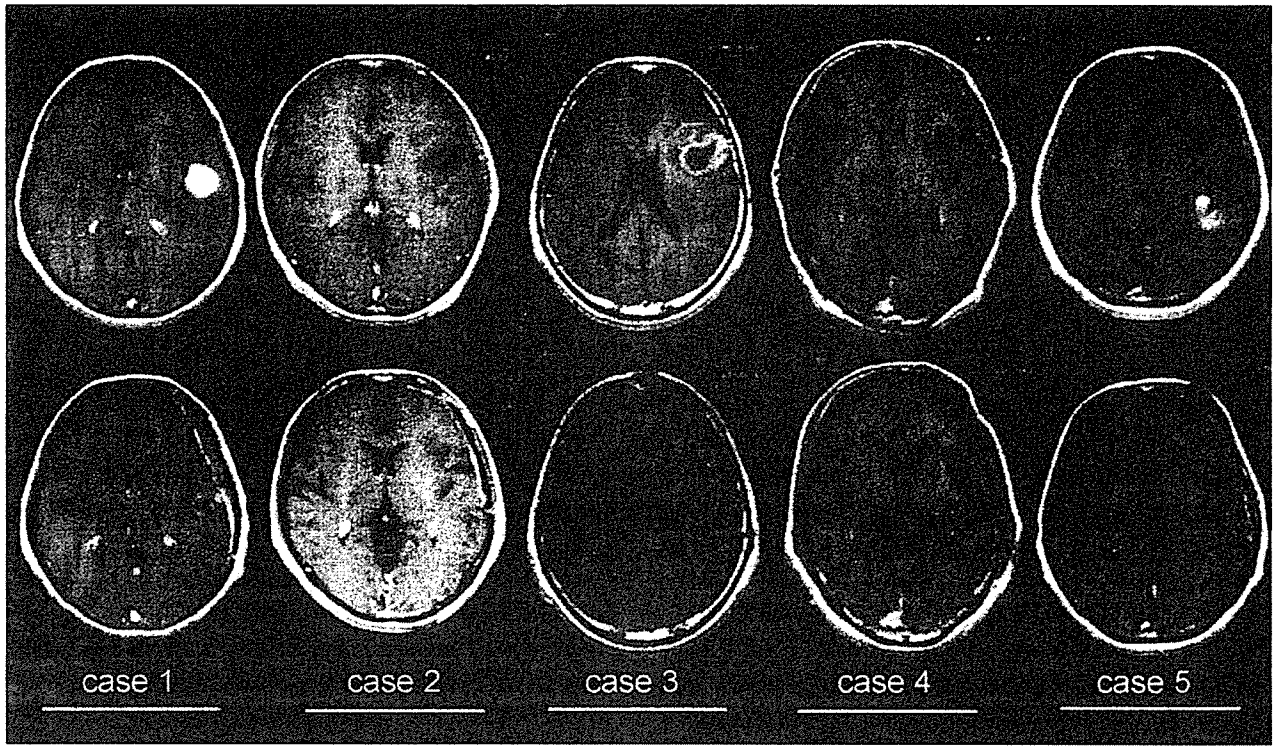

Fig. 6. Pre (*upper line*) – and post (*lower line*)-operative Gd-enhanced, T1-weighted magnetic resonance images obtained on the 5 patients. All tumors were removed almost totally

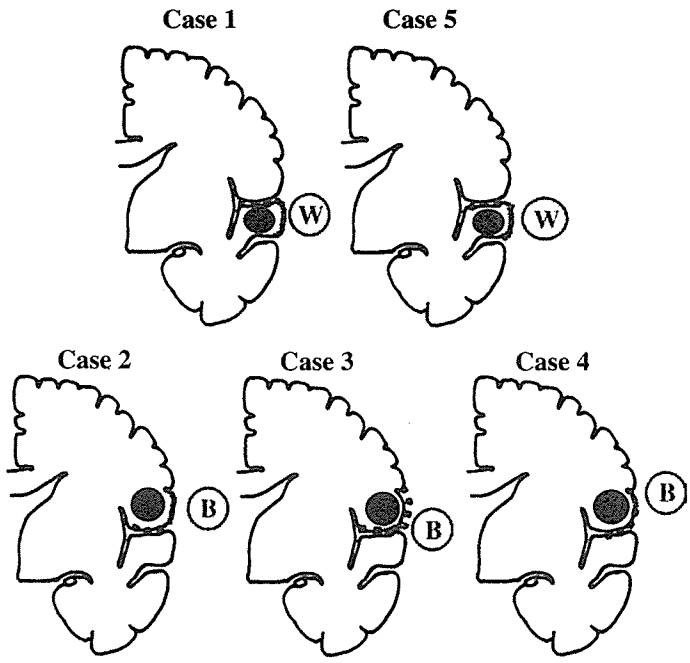

Fig. 7. Schematic drawing of the brain map of the 5 patients. *B* Broca's area, *W* Wernicke's area. The filled circles indicates the tumor. The dotted and gray lines encircle the functional- and non-functional areas, respectively

Discussion

Although functional mapping facilitates the planning of surgery in and around eloquent areas, the resection of tumors adjacent to language areas remains challenging. Ojemann and his associates reported that the essential language area localized to a focal areas of dominant hemisphere cortex of approximately 1 cm^2 [14, 15]. And the exact location of these sites in the left dominant hemisphere was found to vary substantially across the patient

population. Haglund and colleagues reported that a margin of 7 to 10 mm around the language areas resulted in significantly fewer permanent postoperative linguistic deficits [9]. Recently, Duffau and colleagues noted no higher rate of definitive language worsening despite a resection coming in contact with the language sites (but higher rate of transient postoperative aphasia) [4]. Whittle IR *et al.* reported the incidence of iatrogenic dysphasia without intra-operative brain mapping is not dissimilar to that described after resection during use of awake craniotomy and intra-operative language testing [21]. They suggested that a large prospective study would be required to assess the usefulness of intra-operative language testing. Recently, Duffau H *et al.* reported that successful resection of a left insular cavernous angioma using intra-operative language mapping [5]. And Berger MS *et al.* mentioned that to maximize the extent of tumor resection while minimizing permanent language deficits, and recommended the using of cortical stimulation mapping [2]. Although this might be still controversial, we believe intra-operative language mapping is necessary to avoid surgical morbidity.

In this report, we took note that the language areas (Broca's and Wernicke's area) present at the perisylvian fissure. We posit that if there is non-essential language area on the inner surface of the Sylvian fissure, safe tumor resection may be possible even if the tumor is located under the language cortex. We operated on 3 patients with frontal gliomas without new neurological deficit except case 3 who experienced worsening of his aphasia transiently. But, his aphasia was improved 3 months after surgery.

The functional imaging studies allow detection of all the areas implicated in the realization of a task, but not the essential structures in these networks. There has been some work on the importance of the left frontal operculm for syntactic processing [6], and this region is activated during functional imaging studies of language. The functional imaging studies detected the distribution of 'essential' and 'participating' neuronal activity. But, the distribution of 'participating' neurons is substantially different to the focal, lateralized 'essential' sites identified by stimulation mapping for language. Noninvasive functional imaging modalities are an aid to the neurosurgeon, but the golden standard is still believed to be intra-operative monitoring. The evolution of better presurgical functional brain mapping techniques such as magnetic source imaging (MSI), fMRI, and probabilistic Diffuion Tensor imaging/fiber tracking methods will allow an estimation of the anatomical and functional cortex [7, 12]. These techniques may have the potential to promote functional neuronavigation as to an alternative to awake surgery.

The supratemporal plane of the temporal lobe in humans and subhuman primates contains the cortical representation of the primary and association auditory system and forms a part of Wernicke's area. However, the clinical presentation and treatment of patients with lesions in these areas have rarely been described. Silbergeld *et al.* who performed intra-operative cortical mapping during awake surgery on 2 patients subjected to resection of left-hemisphere Heschl gyrus gliomas, reported that neither patient manifested postoperative deficits [18]. Of 3 patients with non-dominant hemisphere Heschl's gyrus gliomas operated on by Russell and Golfinos [17], one presented with postoperative difficulty with music comprehension and production. In this report, we operated on 2 patients with left planum temporale tumors. We only examined language function intra-operatively. However, none of our 2 patients complained of auditory dysfunction and auditory change upon cortical stimulation. And we could remove the tumors without language dysfunction via non-functioning planum temporale cortex.

In our series, 4 of 5 patients had no essential language area on the inner surface of the operculum. Only one patient, a 52-year-old man with a frontal glioblastoma (Case 3) had language function on the inner surface of the frontal operculum. Duffau and colleagues reported 3 cases of inferior frontal gyrus (F3) glioma operated on without neurological deficits. They speculated that total F3 infiltration by glioma, thus a functional reorganization due to brain plasticity would explain the lack of deficit [3]. However, from intra-operative findings, after tumor removal, language cortex replaced on to the surface of the inferior frontal gyrus. We could not detect essential language area on the medial area of the essential language area, and so we speculated his language area was compressed and displaced, rather than that there was reorganization of a new language area.

In conclusion, we posit that there is non-essential language area on the inner surface of the Sylvian fissure. While studies on larger patient populations are necessary, we can remove the perisylvian tumors through overlying non-language cortex. We propose our (opercular) approach may be useful in patients requiring the resection of perisylvian tumors.

Conclusions

Of 5 patients with tumors in the perisylvian cortex, only one, a patient with a frontal glioblastoma, mani-

fested essential language function on the inner surface of the frontal operculum. In this exceptional case, the language cortex was compressed by the tumor and displaced to the inside of the Sylvian fissure. Based on the functional mapping data we obtained, we suggest that even tumors located in the subcortex of the language area may be resectable through the nonfunctioning opercular cortex without inducing postoperative language dysfunction.

References

1. Berger MS, Ojemann GA (1992) Intra-operative brain mapping techniques in neuro-oncology. Streotact Funct Neurosurg 58: 153–161
2. Berger MS, Ojemann GA (1999) Techniques for functional brain mapping during glioma surgery. In: Berger MS *et al* (eds) The Gliomas. W.B. Saunders Philadelphia, pp 421–435
3. Duffau H, Capelle L, Sichez N, Denvil D, Lopes M, Sichez JP, Bitar A, Fohanno D (2002) Intra-operative mapping of the subcortical language pathway using direct stimulations. Brain 125: 199–214
4. Duffau H, Capelle L, Denvil D, Siches N, Gatignol P, Taillandier L, Lopes M, Mitchell MC, Roche S, Muller JC, Bitar A, Sichez JP, van Effenterre R (2003) Usefulness of intra-operative electrical subcortical mapping during surgery for low-grade gliomas located within eloquent brain regions: functional results in a consecutive series of 103 patients. J Neurosurg 98: 764–778
5. Duffau H, Fontaine D (2005) Successful resection of a left insular cavernous angioma using neruonavigation and intra-operative language mapping. Acta Neurochir 147: 205–208
6. Friederici AD, Meyer M, Yves von Cramon D (2000) Auditory language conprehension: An event-related fMRI study on the processing of syntactic and lexical information. Brain and Language 74: 289–300
7. Ganslandt O, Buchfelder M, Hastreiter P, Grummich P, Falbusch R, Nimsky C (2004) Magnetic source imaging supports clinical decision making in glioma patients. Clin Nurol Neurosurg 107: 20–26
8. Hasegawa T, Kishi H, Shigeno K, Tanemura J, Kusunoki K, Kifune Y, Yoshida M (1984) A study on aphasia rating scale: a method for overall assessment of SLTA results. Higher Brain Function Res (Shitsugosyo-Kenkyu) 4: 638–646
9. Haglund MM, Berger MS, Shamseldin M, Lettich E, Ojemann GA (1994) Cortical localization of temporal lobe language sites in patients with gliomas. Neurosurg 34: 567–576
10. Kayama T, Sato S (2001) Definition of individual language related area by awake surgery. No To Shinkei 53: 151–160
11. Mimura M, Kato M, Sano Y, Kojima T, Naeser M, Kashima H (1998) Prospective and retrospective studies of recovery in aphasia. Changes in cerebral blood flow and language functions. Brain 121: 2083–2094
12. Nimsky C, Ganslandt O, Hastreiter P, Wang R, Benner T, Sorensen AG, Fahlbusch R (2005) Preoperative and intra-operative diffusion tensor imaging-based fiber tracking in glioma surgery. Neurosurg 56: 130–138
13. Ojemann SG, Berger MS, Lettich E, Ojemann GA (2003) Localization of language function in children: results of electrical stimulation mapping. J Neurosurg 98: 465–470
14. Ojemann GA (2003) The neurobiology of language and verbal memory: observations from awake neurosurgery. Int J Psychophysiol 48: 141–146
15. Ojemann G, Ojemann J, Lettich E, Berger M (1989) Cortical language localization in left, dominat hemispere. An electorical stimulation mapping investigation in 117 patients. J Neurosurg 71: 316–326
16. Roux FE, Boulanouar K, Lotterie JA, Mejdoubi M, LeSage JP, Berry I (2003) Language functional magnetic resonance imaging in preoperative assessment of language areas: correlation with direct cortical stimulation. Neurosurgery 52: 1335–1345
17. Russell SM, Golfinos JG (2003) Amusia following resection of a Heschl gyrus glioma. Case report. J Neurosurg 98: 1109–1112
18. Silbergeld DL (1997) Tumors of Heschl's gyrus: report of two cases. Neurosurgery 40: 389–392
19. Skirboll SS, Ojemann GA, Berger MS, Lettich E, Winn HR (1996) Functional cortex and subcortical white matter located within gliomas. Neurosurgery 38: 678–684
20. SLTA committee (1997) Standard Language Test of Aphasia: manual of directions. 2nd edn., Homeido, Tokyo
21. Whittle IR, Taylor PR (1998) Effects of resective surgery for left-sided intracranial tumours on language function: a prospective study. The Lancet 351: 1014–1018

Comment

This is an interesting study that emphasizes the value of intra-operative stimulation in awake patients during the resection of lesions adjacent to eloquent cortex. The authors hypothesize that even in the presence of lesions which seem unresectable because of location near Broca's or Wernicke's area, in selected cases a complete resection may be possible when the tumor is approached through a trans-opercular route of non-functional intrasylvian tissue on the inner' surface of the operculum.

In our opinion, however, awake craniotomy, while still regarded as the reference standard of surgery in eloquent cortex, should be considered an interim solution until the advent of better and more powerful functional imaging modalities that help us visualize functionally important brain tissue. We have experience with language MEG (magneto-encephalography) for over 5 years in about 120 cases operated upon for gliomas in the vicinity of Broca' and Wernicke's area with functional neuronavigation. From our experience we conclude that this may well be an alternative to intra-operative awake stimulation.

The evolution of better presurgical functional brain mapping techniques and probabilistic Diffusion Tensor Imaging/fibertracking methods will allow an estimation of the anatomical and functional cortex hitherto norknown. These techniques may have the potential to promote functional neuronavigation as to a true alternative to awake craniotomies. More correlative studies will be warranted in the future to prove that these new techniques are as safe as the proven and tested method of intra-operative electrical stimulation.

References

1. Ganslandt O, Buchfelder M, Hastreiter P, Grummich P, Fahlbusch R, Nimsky C (2004) Magnetic source imaging supports clinical decision making in glioma patients. Clio Neurol Neurosurg 107: 20–26
2. Nimsky C, Ganslandt O, Hastreiter P, Wang R, Boher T, Sorensen AG, Fahlbusch R (2005) Preoperative and intra-operative diffusion tensor imaging-based fiber tracking in glioma surgery. Neurosurgery 56: 130–137

Rudolf Fahlbusch and Oliver Ganslandt
Erlangen

Correspondence: Takamasa Kayama, Department of Neurosurgery, Yamagata University, School of Medicine, 2-2-2 Iidanishi, Yamagata, #990-9585, Japan. e-mail: tkayama@med.id.yamagata-u.ac.jp

皮質てんかんに対する gyrectomy

▣ はじめに

てんかん焦点の切除の眼目は確実な焦点の切除と周囲脳の損傷を避けることである．このために，グリオーマなどの髄内腫瘍摘出法として我々が開発した gyrectomy 法を応用しているので紹介する．

gyrectomy 法

従来，髄内腫瘍の摘出は，図1のごとく，腫瘍に対し subpial にアプローチし，超音波メスや腫瘍鉗子を用いて piece by piece に摘出を進めることが一般的であった．この方法では脳溝内を走行する血管や隣接する脳回の思わぬ損傷や腫瘍の残存を招きかねない．gyrectomy 法は，腫瘍を含み摘出を予定する脳回と周囲の脳回との間の脳溝を開放し，脳溝内の血管や周囲脳回を損傷することなく，腫瘍を含む脳回を一塊として摘出する方法であり，従来の方法の問題を克服することが可能な手技である．

脳溝の開放は摘出する脳回の全周のくも膜を鋏を用いて鋭的に切離しながら，脳表の静脈を隣接する脳回側に寄せていく．くも膜に適度な張力をかけながら，脳溝内を走行する動脈周囲を剝離しながら動脈の走行の把握を進め，摘出する脳回を栄養する動脈を確認したら，その動脈のみを凝固切離する．全周にわたってこれらの操作を脳溝底部まで進めると，摘出する脳回は隣接する脳回と完全に孤立する．最後に脳溝底の深さで脳回を凝固切開し，白質に到達しこれを切離し脳回ごと一塊に摘出する．既に動脈が処理されているため，ほとんど無血下に白質切開を進めることができる．また，腫瘍が底部に残存していても無血下なので視認しやすく，追加切除も容易である(図2)．

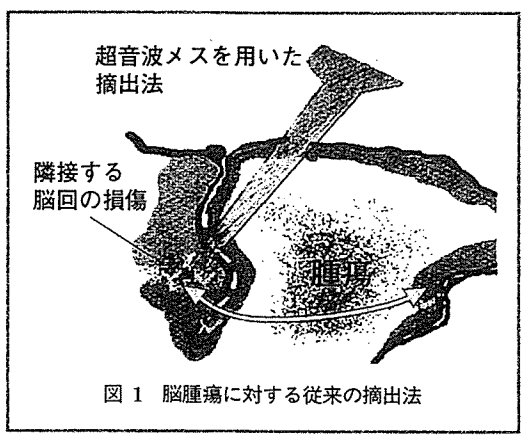

図1　脳腫瘍に対する従来の摘出法

皮質てんかんへの応用

皮質形成異常，結節性硬化症，限局したグリオーマなどで難治てんかんの症例が gyrectomy のよい適応である．これらの病変のように皮質と白質の境界が不鮮明な症例においても確実な摘出が可能であるばかりでなく，隣接する正常な脳回が保護されるため，新たな焦点形成の予防にもなり得，病変の完全な摘出と発作消失の両面で治癒が期待できる．当科では10例の皮質形成性異常病変に対し gyrectomy による焦点切除を行い，全例 Engel の class Ⅰであった．

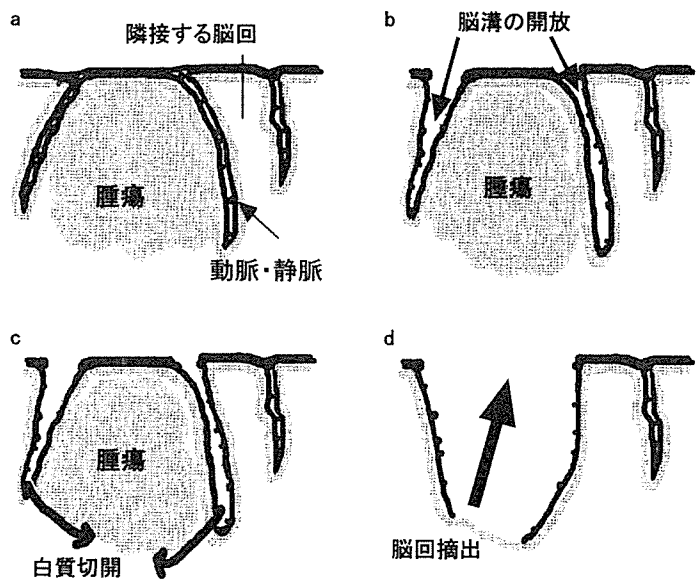

図2　gyrectomy 法の手順

0289-0585/06/¥500/論文/JCLS

櫻田 香 山形大学 脳神経外科
斎藤伸二郎 山形市立病院済生館 脳神経外科
嘉山孝正 山形大学教授 脳神経外科

症 例

9歳女児．6歳時から複雑部分発作と右を向く向反発作と，それに続く全身痙攣発作が出現しだす．フェニトイン 200 mg/日，カルバマゼピン 400 mg/日，フェノバルビタール 500 mg/日を服用していたが，発作は1日に数回は出現していた．MRI にて異常を指摘され当科に紹介となった．皮質脳波記録下に，病変を gyrectomy 法にて一塊として摘出した．摘出標本の病理診断は結節性硬化症に認められる皮質結節であった．術後は発作は一度も出現せず 11 年が経過している(図 3，4)．

▣ ま と め

gyrectomy 法の利点は，1）周囲の脳回および同部を栄養する動脈の不用意な損傷がない，2）腫瘍栄養動脈の選択的で確実な処理を行えるため，無血野での操作が可能となる，3）脳溝底が同定できるため，脳回底部での切除線の決定が容易である，などである．

手術においてはマイクロサージャリーの技術を駆使することには言を俟たないが，摘出脳回の同定，範囲の決定，動脈の処理などには，術前・術中の機能マッピングや術中モニタリング技術の積極的な応用が安全性・確実性をより高めるためには重要である．

文 献

1) 小久保安昭，嘉山孝正，斎藤伸二郎，他．Gyrectomy 法にててんかん焦点を含めて全摘出し得た難治性向反発作を呈した tuberous sclerosis の一手術例．脳外．1997；25：959-64.
2) 丸屋 淳，嘉山孝正，朽木秀雄，他．閃輝暗点発作にて発症し gyrectomy 法にて術中に発作波の消失を確認し得た localized glioma の一例．脳外．1997；25：265-9.
3) Ohki M, Sakurada K, Sonoda Y, et al. Analysis of the extent of astrocytic tumour resection evaluated by magnetic resonance images. Neurosurg Rev. 2003；26：262-5.

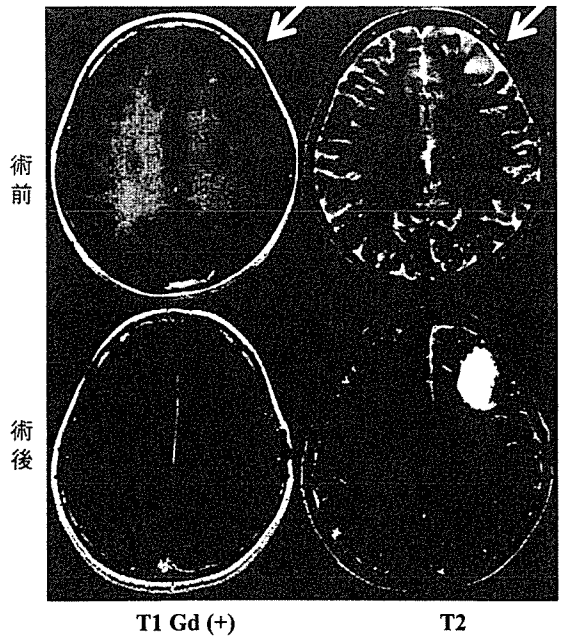

図 3 症例の術前・術後 MRI
病変を含む脳回（矢印）を摘出している．

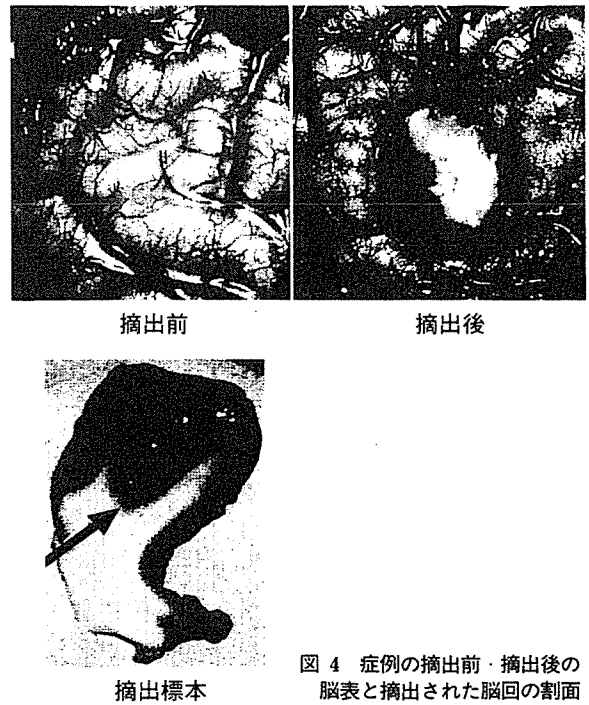

図 4 症例の摘出前・摘出後の脳表と摘出された脳回の割面

Yizhao Chen, M.D., Ph.D.
Department of Neurosurgery,
Graduate School of Medicine,
Kanazawa University,
Kanazawa, Japan and
Department of Neurosurgery,
Graduate School of Medicine,
Kyoto University,
Kyoto, Japan

Osamu Tachibana, M.D., Ph.D.
Department of Neurosurgery,
Graduate School of Medicine,
Kanazawa University,
Kanazawa, Japan

Mitsuhiro Hasegawa, M.D., Ph.D.
Department of Neurosurgery,
Graduate School of Medicine,
Kanazawa University,
Kanazawa, Japan

Ruxiang Xu, M.D., Ph.D.
Department of Neurosurgery,
Pearl River Hospital,
Southern Medical University,
Guangzhou, China

Jun-ichiro Hamada, M.D., Ph.D.
Department of Neurosurgery,
Graduate School of Medicine,
Kanazawa University,
Kanazawa, Japan

Junkoh Yamashita, M.D., Ph.D.
Department of Neurosurgery,
Graduate School of Medicine,
Kanazawa University,
Kanazawa, Japan

Nobuo Hashimoto, M.D., Ph.D.
Department of Neurosurgery,
Graduate School of Medicine,
Kyoto University,
Kyoto, Japan

Jun A. Takahashi, M.D., Ph.D.
Department of Neurosurgery,
Graduate School of Medicine,
Kyoto University,
Kyoto, Japan

Reprint requests:
Jun A. Takahashi, M.D., Ph.D.,
Department of Neurosurgery,
Graduate School of Medicine,
Kyoto University,
54 Shogoin Kawahara-cho, Sakyo-ku,
Kyoto 606-8507, Japan.
Email: jat@kuhp.kyoto-u.ac.jp

Received, August 12, 2005.
Accepted, April 5, 2006.

ABSENCE OF TIGHT JUNCTIONS BETWEEN MICROVASCULAR ENDOTHELIAL CELLS IN HUMAN CEREBELLAR HEMANGIOBLASTOMAS

OBJECTIVE: Endothelial tight junctions form the main barrier of the blood-brain barrier (BBB). In human hemangioblastomas, cyst formation is a common and important clinical manifestation. Although most researchers consider that the cyst formation in hemangioblastomas may be caused by the breakdown of the BBB, the underlying molecular mechanisms for cyst formation remain unknown. At present, there are few reports about the change of tight junctions in microvessel endothelium of human hemangioblastomas. The purpose of this research is to investigate the change of tight junction and its major molecular components in microvessel endothelium of human hemangioblastomas.

METHODS: Twenty-four consecutive patients with cerebellar hemangioblastomas were studied. Tight junctions in the microvessels of hemangioblastomas and the control brain were examined by electron microscopy. Immunohistochemistry and double immunofluorescent microscopy were used to analyze the expression of CLN5 and its relationship with astrocytic endfeet in the control brain and hemangioblastomas. Quantitative real-time reverse-transcriptase polymerase chain reaction and Western blots were used to investigate the expression level of CLN5 in hemangioblastomas. Triple immunofluorescent microscopy was used to analyze the coexpression of vascular endothelial growth factor, vascular endothelial growth factor-R1, and placenta growth factor on microvessels of hemangioblastomas. Clinical and experimental data were correlated and analyzed by the one-way analysis of variance, Kruskal-Wallis test, and Spearman rank correlation test.

RESULTS: In the control brain, the paracellular cleft between adjacent endothelial cells is sealed by continuous strands of tight junctions. In cystic hemangioblastomas, a significant paracellular cleft could be found between adjacent endothelial cells. Some endothelial cells were connected with adherens junction and no tight junction was found between them. Compared with the control brain, expression of CLN5 was decreased in cystic hemangioblastomas ($P < 0.05$). Phosphorylated CLN5 was detected in most hemangioblastomas, but not in the control brain. Microvessels in hemangioblastomas showed a significant absence of astrocytic endfeet. Coexpression of vascular endothelial growth factor, vascular endothelial growth factor-R1, and placenta growth factor was detected in the endothelial cells. The Spearman rank correlation test showed a significant correlation between a greater degree of CLN5 expression and less morphological cystic formation in these patients studied (correlation coefficient = -0.520; $P = 0.009$).

CONCLUSION: The continuity of tight junctions of the BBB is interrupted in human cerebellar hemangioblastomas. Significant absence of astrocytic endfeet and tight junctions can be found in microvessels of hemangioblastomas, which may lead to the breakdown of the BBB in these tumors. These findings suggest that the absence of tight junctions might play a role in cyst formation of hemangioblastomas.

KEY WORDS: Blood-brain barrier, Cyst, Hemangioblastoma, Tight junction

Neurosurgery 59:660-670, 2006 DOI: 10.1227/01.NEU.0000223372.18607.D7 www.neurosurgery-online.com

Hemangioblastomas (HBs) account for 1 to 2.5% of all primary central nervous system (CNS) neoplasms and approximately 7% of primary posterior fossa tumors in adults (25, 29). In these tumors, cyst formation is a common and important clinical manifestation. Most mass effect-producing symptoms in cystic HB patients derive from the cyst rather than from the tumor causing the cyst (35). Although most researchers consider that the cyst formation in HBs may be caused by the breakdown of the blood-brain barrier (BBB) for an extended period (12, 23), the exact molecular basis and the pathophysiological process remain unknown.

The BBB is a physical and metabolic barrier between the CNS and the systemic circulation that regulates and protects the microenvironment of the brain (17). In the BBB, endothelial tight junctions (TJs) form the main barrier (11, 39). The formation of TJs between endothelial cells (ECs) is a basic microvascular feature in the CNS that results in high transendothelial electrical resistance (1500–2000 $\Omega \times cm^2$) and decreased paracellular permeability (6). Disruption of TJs in the BBB has been found in some human tumors (5, 8, 27). At present, there are few reports about the change of TJs in microvessel endothelium of human HBs. Recently, it has been found that a TJ is composed of many molecular components, such as claudins and occludins. Decreased expression of TJ proteins has been shown to be related to the increased microvascular permeability in human gliomas (21, 30, 42). The aim of this study was to investigate the change in TJs and their major molecular components in the microvessel endothelium of human HBs.

PATIENTS AND METHODS

Patient Population and Imaging

We examined 24 consecutive patients with cerebellar HBs (11 women, 13 men) treated at our institutions between 1980 and 2005. The mean age of the patients at the time of presentation was 42.3 ± 15.5 yr. Of the 24 patients, six were diagnosed with von Hippel-Lindau disease (VHL) according to family histories.

All computed tomographic and magnetic resonance imaging scans of the patients were evaluated separately by two authors (YC, OT) for HBs and associated cysts. To evaluate the cyst formation of HBs, all tumors were classified into three grades according to the macroscopic pattern of each tumor: Grade 1 (Group 1) corresponded to macroscopic solid tumor; Grade 2 (Group 2) to a mainly solid tumor with macroscopic cysts; and Grade 3 (Group 3) to a cystic neoplasm with a small tumor nodule located in the cyst wall (33). HBs in Groups 2 and 3 were considered cystic HBs.

Surgical Tissue Specimens

Twenty-four paraffin-embedded HB specimens were obtained from patients undergoing therapeutic removal of tumors and were used for immunohistochemical study. Nine fresh frozen samples collected between 1997 and 2005 were flash-frozen immediately after removal and stored at −136°C. Histological diagnosis was confirmed through standard light microscopy evaluation of sections stained with hematoxylin and eosin. All of the tumor tissues in the present study were obtained from primary resections. Control brain specimens were obtained from the cortex of temporal lobe of five epilepsy patients who were treated by temporal lobectomy and the cerebellar tissue of a patient with low-grade brainstem astrocytoma who was treated by surgery.

Electron Microscopy

Electron microscopy was performed in 10 HBs and four control brain specimens that were collected between 1990 and 2005 at our institution. Surgically extracted specimens were fixed in phosphate buffer containing 2% glutaraldehyde and were immediately cut into small fragments (approximately 1 mm^3). After postfixation with 1% OsO_4 in 0.1 mol/L phosphate buffer (pH, 7.4), specimens were processed according to the standard method and were embedded in Epon 812. Ultrathin sections were stained with uranyl acetate and lead citrate and were examined using an electron microscope (H71-FA; Hitachi, Ltd., Tokyo, Japan). Images were recorded on standard transmission electron microscopy film and were subsequently digitized using a digital scanner (ES-2200; Epson, Tokyo, Japan). In each section, a total of 10 microvessels were randomly chosen and examined under a transmission electron microscope. Microvessels with an absence of intercellular TJs were labeled and recorded. The exact percentage of microvessels with absence of intercellular TJs in all microvessels was calculated.

Extraction of Ribonucleic Acid and Conventional Reverse-transcriptase Polymerase Chain Reaction Analysis

Ribonucleic acid (RNA) was extracted from nine fresh frozen HBs and control brain specimens using RNeasy kit (Qiagen, Hilden, Germany) according to the supplier's protocol. Conventional reverse-transcriptase polymerase chain reaction (RT-PCR) was performed using Ready-To-Go RT-PCR Beads (Amersham Biosciences Corp., Piscataway, NJ). The primer pair used to detect claudin 5 (CLN5) messenger RNA (mRNA) was as follows: 5′-TAA GCA GAT TCT TAG CCT T-3′ (upstream) and 5′-GTG TAC AGC TGG TCT TTA CT-3′ (downstream), with an expected PCR product of 157 bp. For the control gene encoding β-actin, the primers 5′-CTA CAA TGA GCT GCG TGT GGC-3′ (upstream) and 5′-CAG GTC CAG ACG CAG GAT GGC-3′ (downstream) were used, with an expected PCR product of 271 bp. After reverse transcription at 42°C for 30 minutes, amplifications were performed for 30 cycles under the following conditions: denaturation, 94°C for 30 seconds; annealing, 50°C for 45 seconds; and extension, 72°C for 1 minute. PCR products were separated on 2% agarose gels and were visualized with ethidium bromide staining. An HB sample was analyzed without reverse transcriptase as a negative control.

Quantitative Analysis of CLN 5 mRNA

Real-time RT-PCR was performed using a Quantitect Reverse Transcription Kit (Qiagen) and fluorescence thermocycler (LightCycler; Roche Diagnostics GmbH, Mannheim, Germany). Relative quantification based on the β-actin mRNA levels was used to determine the amount of CLN5 mRNA in HBs and control brain specimens. After extraction, RNA sample was incubated briefly in genomic deoxyribonucleic acid (DNA) Wipeout Buffer (Qiagen) at 42°C for 2 minutes to effectively remove contaminating genomic DNA. The complementary DNA corresponding to 10 ng RNA served as a template in a 20-μl reaction containing 0.5 μmol/L for each primer, deoxynucleoside triphosphate mix, and QuantiTect SYBR Green PCR Master Mix (Qiagen). Samples were loaded into capillary tubes and were incubated in the fluorescence thermocycler (LightCycler) for an initial denaturing at 95°C for 10 minutes, followed by 35 cycles, with each cycle consisting of 95°C for 15 seconds, 50°C for 30 seconds, and 72°C for 30 seconds. Finally, the temperature was raised gradually (0.1°C/s) from the annealing temperature to 95°C for the melting curve analysis. Cycle-to-cycle fluorescence emission readings were monitored and analyzed using LightCycler Software (Roche Molecular Biochemicals). Relative CLN5 mRNA levels based on the β-actin mRNA levels were calculated and normalized. An HB sample without reverse transcription was analyzed as a negative control.

Immunohistochemical Analysis

All paraffin-embedded specimens were fixed in buffered formalin and saline and were processed into paraffin wax. Tissue sections (5 μm) mounted on MAS-coated slides (Matsunami Glass, Inc., Osaka, Japan) were deparaffinized by treatment in xylene twice, rehydrated in a graded ethanol series, and rinsed in phosphate-buffered saline (PBS) (pH, 7.4). Antigen retrieval was performed by boiling (750 W) in citric acid buffer (10 mmol/L, pH 6.0) for 5 minutes in a microwave oven. The sections were allowed to cool to room temperature in the buffer and were then rinsed in PBS (pH, 7.4). The endogenous peroxidase activity was blocked in 0.3% hydrogen peroxide in methanol for 30 minutes. Thereafter, the sections were incubated with normal serum for 30 minutes (VECTASTAIN elite ABC KIT; Vector Laboratories, Burlingame, CA). Incubation with monoclonal mouse anti-CLN5 antibody (18-7364; Zymed Laboratories, South San Francisco, CA) and anti–vascular endothelial growth factor (VEGF) antibody (SC-7269, Santa Cruz Biotechnology, Santa Cruz, CA) took place overnight at 4°C followed by antimouse biotinylated antibody and VECTASTAIN ABC Reagent (Vector Laboratories). All slides were then developed in 3, 3′-diaminobenzidine tetrahydrochloride (Vector Laboratories) for 4 minutes. After rinsing in distilled water, sections were counterstained with hematoxylin. Finally, the sections were dehydrated, cleared in xylene, and mounted in ENTELLAN (Merck KgaA, Darmstadt, Germany). Expression of CLN5 on microvascular ECs were graded as –, +, or ++ by two histopathologists who were blinded to all clinical information on the specimens.

Fluorescent Immunostaining and Confocal Microscopy

After deparaffinization, rehydration, and antigen retrieval, tissue sections were incubated in donkey serum (Chemicon International, Temecula, CA) for 1 hour at room temperature. To detect the astrocytic endfeet and CLN5 expression on microvessel endothelium, coincubation with monoclonal mouse anti-CLN5 antibody (18-7364; Zymed) and polyclonal rabbit antiglial fibrillary acidic protein (GFAP) antibody (Z0334; DakoCytomation, Copenhagen, Denmark) took place overnight at 4°C. Sections were washed with PBS and were incubated with Alexa Fluor donkey antimouse 594 and donkey antirabbit 488 secondary antibodies (Molecular Probes, Eugene, OR) for 1 hour at 37°C. To investigate the coexpression of VEGF, VEGF-R1 (Flt-1), and placenta growth factor (PIGF), coincubation with monoclonal mouse anti-VEGF antibody (SC-7269; Santa Cruz Biotechnology), polyclonal rabbit anti-Flt-1 antibody (SC-316; Santa Cruz Biotechnology) and polyclonal goat anti-PIGF antibody (SC-6164; Santa Cruz Biotechnology) took place overnight at 4°C. Sections were washed with PBS and were incubated with Alexa Fluor donkey antimouse 594, donkey anti-rabbit 488, and Alexa Fluor donkey anti-goat 350 secondary antibodies (Molecular Probes) for 1 hour at 37°C. Then, all slides were covered with UltraCruz Mounting Medium (Santa Cruz Biotechnology). Photomicrographs were obtained using an AX80 microscope (Olympus Optical Co., Tokyo, Japan) and Olympus Fluoview Confocal Microscope (Olympus Optical Co.).

Western Blots

Fresh frozen samples were homogenized in buffer (62.5 mmol/L Tris HCl, pH 7.6, 2% sodium dodecyl sulfate, 10% glycerol, 1 mmol/L dithiothreitol, 0.01% bromophenol blue, and 2% mercaptoethanol) and centrifuged at 10,000 x *g* for 5 minutes at 4°C. Protein concentration was determined by Bradford assay (Bio-Rad, Hercules, CA). After being boiled for 2 minutes, 10 μg of each sample were loaded onto 12% polyacrylamide Tris-HCl gels (Bio-Rad) and run at 40 mA for 70 minutes at 4°C. Proteins then were transferred onto Hybond-P polyvinylidene fluoride membranes (Amersham Biosciences Corp). After incubation in blocking buffer consisting of 50 mmol/L Tris HCl (pH 7.4), 150 mmol/L NaCl (Tris-buffered saline), 0.1% Tween 20, and 5% bovine serum albumin for 1 hour at room temperature, membranes then were rinsed once in Tris-buffered saline and were treated with antibodies CLN5 and β-tubulin (Sigma-Aldrich, Inc., St. Louis, MO) overnight at 4°C. Membranes were rinsed three times in Tris-buffered saline and 0.1% Tween 20 at room temperature and were incubated for 1 hour with ECL-HRP linked antimouse immunoglobulin G (Amersham Biosciences Corp). The membrane was washed and then drained to remove excess liquid. Detection of the protein of interest was obtained by chemiluminescence detection using ECL Plus Western blotting detection

reagents from Amersham Pharmacia Biotech (Piscataway, NJ). For detection of each reaction, 4 ml ECL Plus solution A and 0.1 ml ECL Plus solution B were mixed together and quickly poured over the moist membrane. The membrane was enclosed in a piece of cling film and was exposed to Hyperfilm (Amersham Pharmacia Biotech) using different exposure times to optimize the signal. The exposed Hyperfilms were developed using an automated photoimage developer system.

Statistical Analysis

A one-way analysis of variance was used to analyze the normalized expression level of CLN5 mRNA and the proportion of microvessels with absence of intercellular TJs among different clinical groups. If a significant analysis of variance was found, post hoc tests (Student's, Newman-Keuls, and least significant difference tests) controlling for multiple comparisons were used to identify pairs of diagnostic groups that differed significantly. Nonparametric Kruskal-Wallis tests were used to evaluate the immunohistochemical results of CLN5 among different groups. A Spearman rank correlation test for nonparametric data was used to analyze the correlation between the degree of CLN5 expression on ECs and the macroscopic pattern of the tumors. All of the data were analyzed using a commercially available statistical package (SPSS, version 11.01; SPSS, Inc., Chicago, IL). A probability value less than 0.05 was taken as the level of significance.

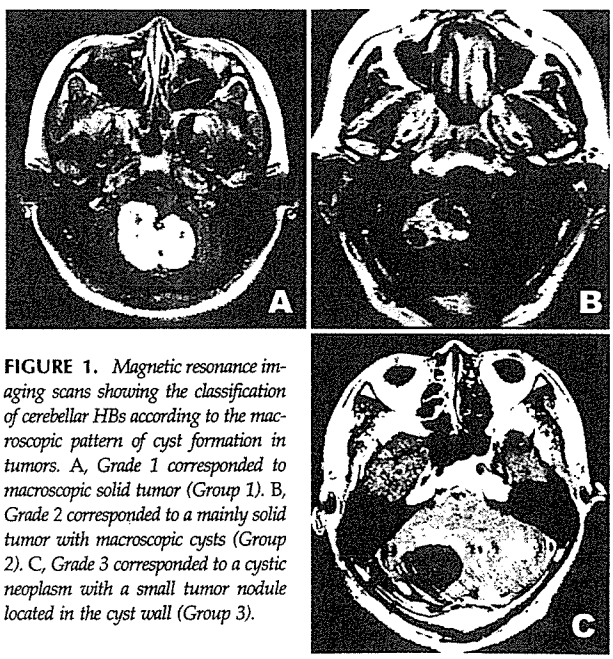

FIGURE 1. *Magnetic resonance imaging scans showing the classification of cerebellar HBs according to the macroscopic pattern of cyst formation in tumors.* A, *Grade 1 corresponded to macroscopic solid tumor (Group 1).* B, *Grade 2 corresponded to a mainly solid tumor with macroscopic cysts (Group 2).* C, *Grade 3 corresponded to a cystic neoplasm with a small tumor nodule located in the cyst wall (Group 3).*

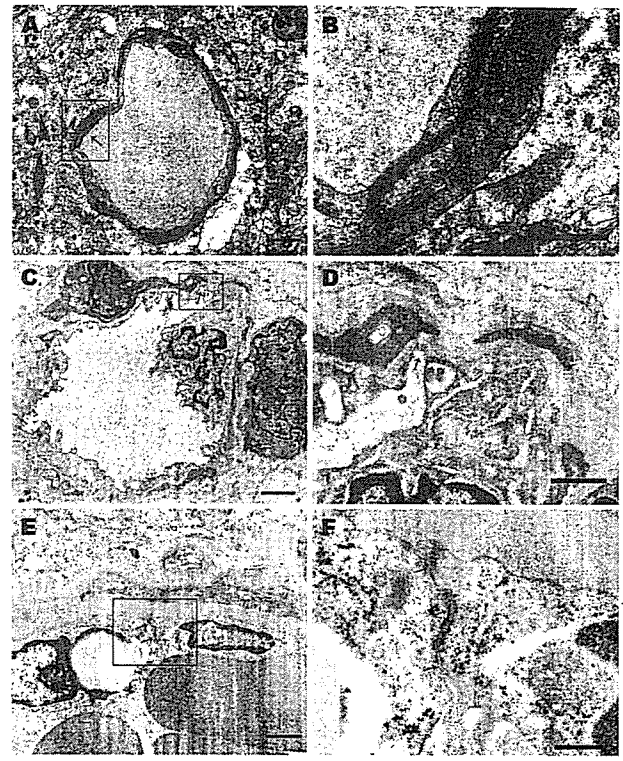

FIGURE 2. *Electron microscopy images of control brain and HBs.* A, *in control brain, a paracellular cleft between adjacent ECs is sealed by continuous strands of TJs. No fenestration is found in the endothelium of control brain* (arrows *indicate TJ;* scale bar, *1.5 μm).* B, *under higher magnification, continuous TJs were seen clearly between adjacent ECs* (arrows *indicate TJ;* scale bar, *0.2 μm).* C, *paracellular clefts between adjacent ECs were found in HBs* (arrow; scale bar, *1.5 μm).* D, *under higher magnification, a paracellular cleft between adjacent ECs was seen clearly in HBs* (arrow; scale bar, *0.6 μm).* E, *adjacent ECs were connected with adherens junction (arrows).* Scale bar, *1.5 μm.* F, *under higher magnification, an AJ* (arrows) *was seen clearly and no TJ was found between them* (Scale bar, *0.3 μm).*

RESULTS

Demographic Data

In this study, we analyzed 24 HBs that were localized within the cerebellum. According to the preoperative computed tomographic and magnetic resonance imaging scans and intraoperative findings, six HBs (25.0%) showed a macroscopic solid pattern (one patient had VHL disease, Grade 1, *Fig. 1A*). Cyst formation of Grade 2 was found in nine HBs (VHL disease, Grade 2, *Fig. 1B*). The remaining nine HBs (three patients had VHL disease) showed a macroscopic cystic pattern (*Fig. 1C*, Grade 3). No significance was found between the cyst formation of sporadic HB and VHL disease ($P > 0.05$).

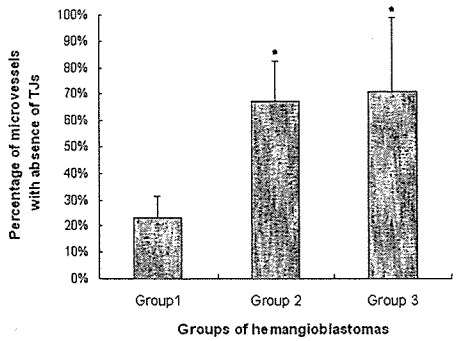

FIGURE 3. *Bar graph showing the absence of TJs in microvessels of HBs. In cystic HBs (Groups 2 and 3), the absence of intercellular TJs was found in 67.3% of microvessels in Group 2 and in 71.0% of microvessels in Group 3. Compared with cystic HBs, the absence of intercellular TJs was found less frequently in solid HBs (Group 1).* Asterisk, $P < 0.05$).

Electron Microscopy

In the control brain, all paracellular clefts between adjacent ECs were sealed by continuous strands of TJs. No fenestration was found in the endothelium of the control brain (*Fig. 2A*). Under higher magnification, continuous TJs were clearly seen between adjacent ECs (*Fig. 2B*). In HBs, an absence of intercellular TJs was found in 67.3% of microvessels in Group 2 and 71.0% of microvessels in Group 3. Compared with cystic HBs (Groups 2 and 3), absence of intercellular TJs was found less frequently in solid HBs (Group 1, $P < 0.05$). Only 23.3% of microvessels in solid HBs showed absence of intercellular TJs. These results are shown in *Figure 3*. *Figure 2, C* and *D* show the paracellular cleft between adjacent ECs and TJs between adjacent ECs that were interrupted in microvessels. Significant fenestrations were found in the endothelium of HBs (*Fig. 2C*). *Figure 2, E* and *F* show the adherens junction between adjacent ECs; no TJ was found between them. Residual, relatively intact TJs could be found in some area of tumor tissues.

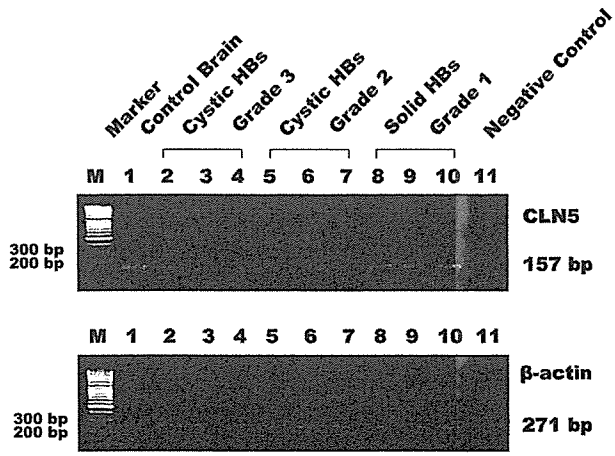

FIGURE 4. *PT-PCR analysis showing representative conventional RT-PCR results of human HBs and control brain specimens. RT-PCR analysis revealed a strong expression of CLN5 in control brain* (Lane 1). *Expression of CLN5 was decreased significantly in cystic HBs (Groups 2 and 3,* Lanes 2–7). *Solid HBs (Group 1,* Lanes 8–10) *showed a higher expression of CLN5 compared with cystic HBs. The HB sample was analyzed without reverse transcriptase as a negative control* (Lane 11). *Human β-actin (271-bp PCR product) was amplified as an internal control.* M, *marker.*

Conventional RT-PCR and Quantitative Real-time RT-PCR Analysis

We used genomic DNA Wipeout Buffer (Qiagen) to eliminate possible genomic DNA contamination. Both conventional RT-PCR and real-time RT-PCR were used to analyze the expression level of CLN5 mRNA. Representative conventional RT-PCR results of human HBs and control brain specimens are shown in *Figure 4*. *Figure 5* shows our real-time RT-PCR results of CLN5 in control brain and HBs. Compared with solid HBs and control brain, CLN5 expression was decreased significantly in cystic HBs (Groups 2 and 3; $P < 0.05$). Solid HBs (Group 1) showed a higher expression level of CLN5 mRNA than that of control brain in our experiments, although no significant difference was found between them ($P = 0.22$, least significant difference test). These results are shown in *Figure 5*. To analyze the expression and possible phosphorylation of CLN5 protein, we performed immunohistochemical and Western blot analysis.

Immunohistochemical Analysis

To detect the expression and distribution of CLN5 in control brain and HBs, immunohistochemical analysis of paraffin-embedded tissue sections was performed. In control brain tissue, strong expression of CLN5 could be found on microvascular ECs (*Fig. 6C*). In histopathological analysis, HBs are characterized by two main components: large vacuolated stromal cells and a rich capillary network (*Fig. 6B*). *Figure 6D*, from a cystic HB, shows

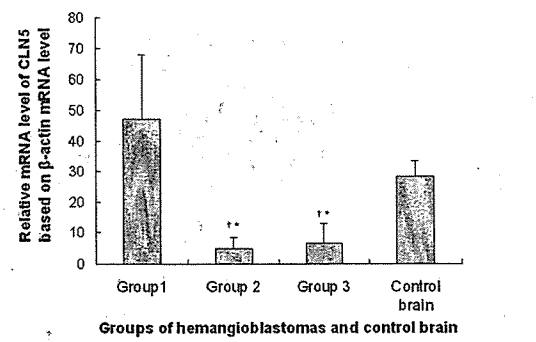

FIGURE 5. *Bar graph showing quantitative analysis of CLN5 mRNA in human HBs and control brain specimens by real-time RT-PCR. Compared with solid HBs and control brain, CLN5 expression was significantly decreased in cystic HBs (Groups 2 and 3; $P < 0.05$). Solid HBs (Group 1) showed a higher expression level of CLN5 mRNA than that of control brain in our experiments, although no significant difference was found between them. ($P = 0.22$).* Asterisk, $P < 0.05$ *compared with control brain.* †, $P < 0.05$ *compared with solid HBs (Group 1).*

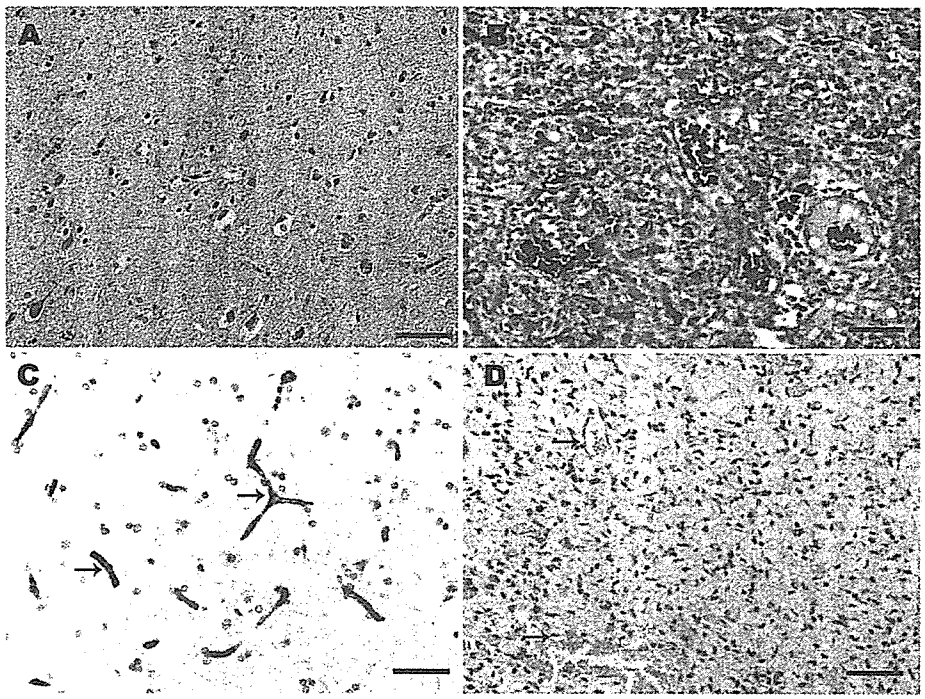

FIGURE 6. *Photomicrographs revealing representative immunohistochemical results of CLN5 expression in HBs and control brain specimens.* A, *control brain (hematoxylin and eosin).* B, *typical histological characteristics of HB with large vacuolated stromal cells and a rich capillary network (hematoxylin and eosin).* C, *strong expression of CLN5 was detected on endothelium of the control brain* (arrows). D, *expression level of CLN5 was decreased in microvascular ECs of cystic HBs* (arrows). Scale bars, 25 μm.

TABLE 1. Summary of claudin 5 expression in endothelium of human cerebellar hemangioblastomas and control brain[a]

Expression of CLN5 in ECs	Control brain	Cyst formation of HBs		
		Grade 1	Grade 2	Grade 3
Negative	0	1	0	5
Positive	0	0	3	2
Double positive	6	5	6	2
Total cases	6	6	9	9

[a] CLN5, claudin 5; ECs, endothelial cells; HBs, hemangioblastomas.

the dramatically decreased expression of CLN5 in microvessel endothelium of a cystic HB.

These results are summarized in *Table 1*. We analyzed the results of immunohistochemical staining combined with the clinical data from our patients to determine whether expression of CLN5 correlated with cyst formation in HBs. Compared with the control brain, expression of CLN5 was decreased in cystic HBs ($P < 0.05$). A significant difference in CLN5 expression was found between cystic HBs and solid HBs ($P = 0.025$). The Spearman rank correlation test showed a significant correlation between a greater degree of CLN5 expression and less morphological cystic formation in the patients studied (correlation coefficient = −0.520; $P = 0.009$). These results were in accordance with our quantitative real-time RT-PCR results. To confirm the expression of CLN5 and its relationship with the astrocytic end-feet of BBB, we used double immunofluorescent staining of CLN5 and GFAP to analyze their expression in the BBB.

Immunofluorescence Microscopy for CLN5 and GFAP

We used polyclonal rabbit antihuman GFAP antibody to label astrocytic endfeet and to analyze the relationship between astrocytic endfeet and CLN5 expression in the BBB of the control brain and HBs. In the control brain, astrocytic endfeet visualized by GFAP staining ensheathed the microvessels (*Fig. 7, A* and *C*). CLN5 is expressed strongly in microvascular ECs (*Fig. 7, B* and *C*). In most HBs, there is a significant absence of astrocytic endfeet in their microvessels (*Fig. 7, D* and *F*). Gliosis was found in tumor tissues (*Fig. 7D*). Expression of CLN5 was decreased in microvascular ECs (*Fig. 7, E* and *F*).

Coexpression of VEGF, Flt-1, and PlGF in HBs

VEGF is a potent mediator of capillary leak. The expression level of VEGF is relatively low in control brain (*Fig. 8A*). Overexpression of VEGF could be found in human HBs (*Fig. 8B*). To investigate the possible role of coexpression of angiogenic factors in the absence of TJs in HBs, we used triple immunofluorescent staining of VEGF, Flt-1, and PlGF in HBs. Compared with negative expression of VEGF, Flt-1, and PlGF in control brain (*Fig. 9, A–D*), positive expression of VEGF (*Fig. 9F*) and PlGF (*Fig. 9G*) were found on both stromal cells and ECs. *Figure 9E* shows that Flt-1 expression is positive in ECs of HBs. Coexpression of VEGF, Flt-1, and PlGF was found in ECs of HBs (*Fig. 9H*).

Western Blot Analysis

To investigate the expression level of CLN5 protein, we used Western blot analysis to confirm our previous results. In control brain, a strong expression of CLN5 protein was detected. *Figure 10* shows that the expression level of CLN5

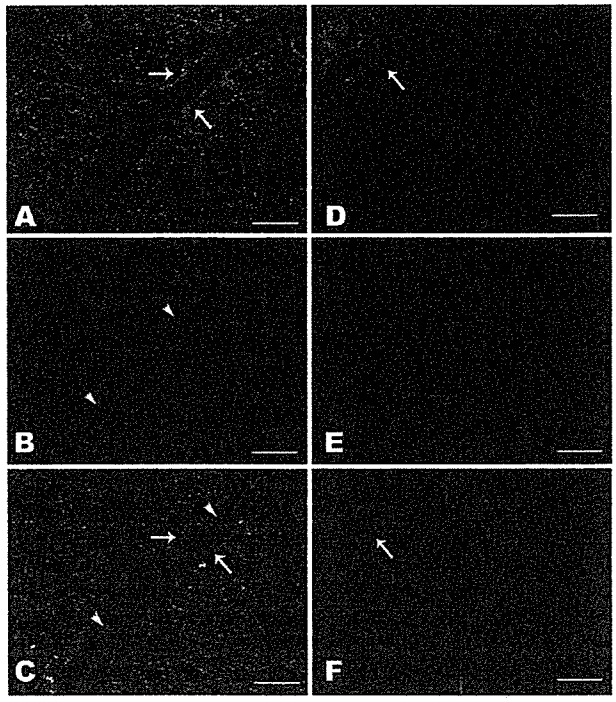

FIGURE 7. *Photomicrographs showing immunofluorescence in the control brain and HBs stained with GFAP* (green) *and CLN5* (red). A, *positive GFAP detected on astrocytes of control brain* (arrow). B, *strong expression of CLN5 was detected on the endothelium of the control brain* (arrowhead). C, *merge of* A *and* B. *Microvascular ECs in the control brain showed a strong expression of CLN5* (arrow). *Astrocytic endfeet visualized by GFAP staining ensheathed the microvessels* (arrow). D, *gliosis stained by GFAP in HBs* (arrow). E, *microvascular ECs are negative for CLN5 staining. Note the red blood cells within microvessels.* F, *merge of* D *and* E. *In cystic HBs, there is a significant absence of astrocytic endfeet in their microvessels. Gliosis was found in tumor tissues* (arrow). *Expression of CLN5 was decreased in microvascular ECs.* Scale bars, *25 μm*

protein was dramatically decreased in cystic HBs (Groups 2 and 3) in comparison with control brain. Solid HBs (Group 1) showed a higher expression of CLN5 than cystic HBs (Groups 2 and 3). Phosphorylated CLN5 was detected in most HBs, including both solid and cystic HBs, but not in control brain. This result was in accordance with our previous experimental results.

DISCUSSION

Cyst formation is commonly associated with cerebellar, brainstem, and spinal HBs. Most (60–70%) of all cerebellar HBs are cystic masses (18, 44). Moreover, the pace of enlargement is much faster for cysts than for HBs themselves (35, 43). As a result, it is the cysts that mainly cause the mass effect-producing symptoms in patients of cystic-type HBs (35). At present, most researchers consider the cyst formation in HBs to be a result of the breakdown of the BBB (12, 23). In cystic fluid, more than 92% of total cyst fluid protein consists of plasma protein fractions. This implies that the greater part of the cyst fluid proteins must derive from plasma, and the cyst formation in brain tumors could be associated with the breakdown of the BBB (12, 22). However, there is little evidence regarding the exact pathophysiological mechanism and molecular basis for cyst formation in HBs. This prompted us to investigate changes in TJs and the major molecular components in microvessels of HBs.

The BBB is a diffusion barrier essential for the homeostatic regulation of the brain microenvironment and normal function of the CNS (3). The BBB is composed of three cellular elements: ECs, astrocyte endfeet, and pericytes. In the BBB, capillary ECs are connected together with continuous TJs (4, 13, 37). The formation of TJs produce a barrier to inhibit the paracellular transport between cerebral ECs. Among all cellular elements of the BBB, endothelial TJs are recognized as the anatomic substrate of the BBB (11, 39). Astrocyte endfeet tightly ensheathe the vessel wall. They are speculated to be critical for the induction and maintenance of the TJ barrier (3). In this study, our results showed that the continuity of TJs of microvessels was interrupted in human cerebellar HBs. Compared with the continuous TJs in the control brain, some capillary ECs of HBs were connected with only adherens junction and no TJ could be found between them. A paracellular cleft frequently was found between adjacent ECs in HBs. Compared with solid HBs, absence of TJs was found much more frequently in microvessels of cystic HBs. These results in combination with the absence of astrocytic endfeet provided us with the morphological evidence of a

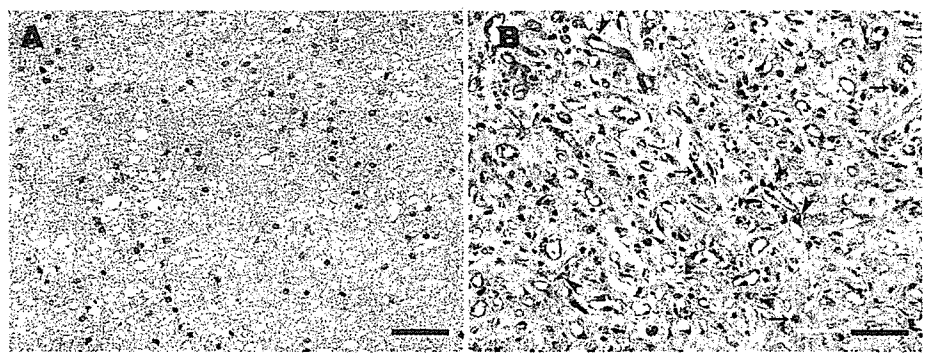

FIGURE 8. *Photomicrographs showing VEGF expression in the control brain and HBs.* A, *VEGF expression is negative in the control brain.* B, *overexpression of VEGF could be found in HBs. VEGF is positive both in stromal cells* (arrows) *and microvascular ECs* (arrowheads). Scale bars, *50 μm.*

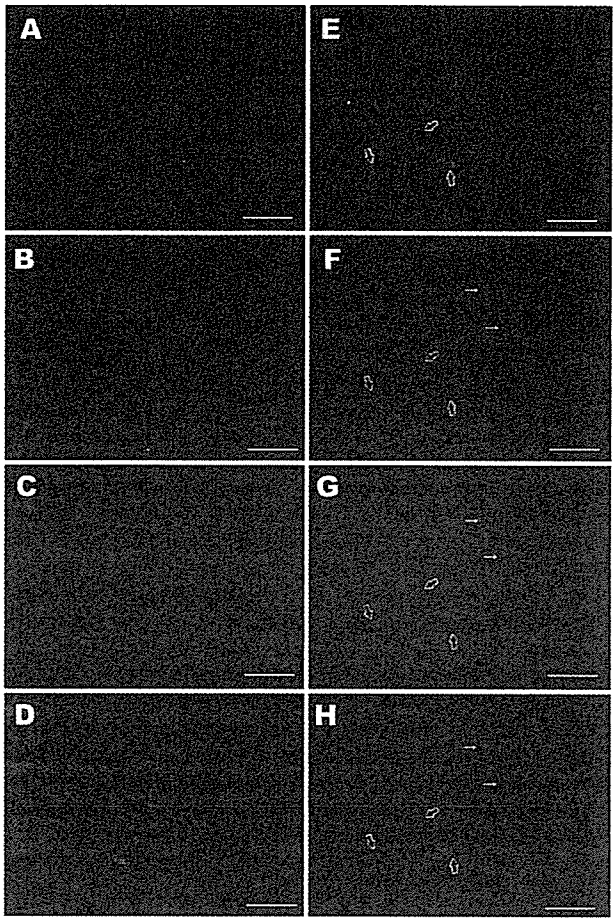

FIGURE 9. *Photomicrographs showing coexpression of VEGF, Flt-1, and PIGF in HBs and the control brain.* A, *Flt-1 expression in the control brain.* B, *VEGF expression in the control brain.* C, *PIGF expression in the control brain.* D, *merge of* A–C. No coexpression of VEGF, Flt-1, and PIGF was detected in microvascular ECs of the control brain. E, *Flt-1 expression* (green) *is positive in ECs of HBs* (arrows). F, *VEGF expression* (red) *is positive both in stromal cells* (arrows) *and microvascular ECs* (open arrows) *of HBs.* G, *positive PIGF* (blue) *evidence could be found in stromal cells* (arrows) *and microvascular ECs* (open arrows) *of HBs.* H, *merge of* E–G. *Coexpression of VEGF, Flt-1, and PIGF was detected in microvascular ECs of HBs* (open arrows). Scale bars, *25 μm.*

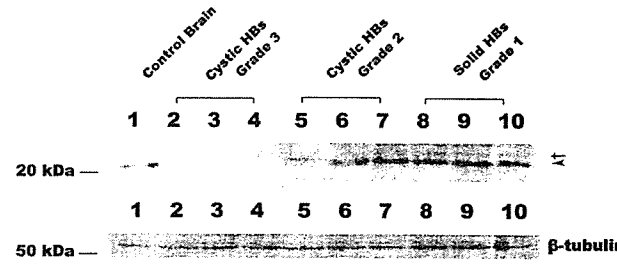

FIGURE 10. *Western blot analysis of CLN5 protein expression in human cerebellar HBs and the control brain. A strong expression of CLN5 was found in the control brain* (Lane 1). *The expression level of CLN5 was significantly downregulated in cystic HBs (Groups 2 and 3,* Lanes 2–7). *Solid HBs (Group 1,* Lanes 8–10) *showed a higher expression of CLN5 than cystic HBs. Phosphorylated CLN5* (arrow) *was detected in most HBs including both solid and cystic HBs but not in the control brain. The* arrowhead *indicates the position of CLN5 without phosphorylation; the* arrow *indicates the position of phosphorylated CLN5.*

breakdown of the BBB in HBs, suggesting that the absence of TJs in microvessels may play a role in cyst formation of HBs.

TJs are composed of several molecular components, including CLNs, occludin, junctional adhesion molecule, and zonula occludens (14). In this study, although we did not find significant changes of expression of occludin, zonula occludens-1, and junctional adhesion molecule (data not shown), the CLN5 expression level unexpectedly showed a significant decrease in ECs of cystic HBs. Furthermore, the Spearman correlation test showed a correlation between a greater degree of CLN5 expression and less morphological cystic formation in HBs. These results are in accordance with our previous ultrastructural findings of TJs in HBs. In the BBB, CLN5 is a major cell adhesion molecule of TJs in cerebral ECs (14, 26). Compared with other TJ proteins, CLNs are necessary and sufficient for the formation of TJs (10, 16, 26). Decreased expression of CLN5 has been proven to play a crucial role in increased vascular permeability in many human diseases. In human brain, downregulation of CLN5 was found to be related to the increase in microvascular permeability and brain edema in gliomas (21). Interestingly, it has been demonstrated that the development of cysts is related to brain edema in gliomas (35). There is histological evidence of a gradual liquefaction of the spongy edematous tissue that form the cyst fluid (35). Therefore, it is suggested that the dysregulation of CLN5 may play a role in the breakdown of the BBB and cyst formation of human HBs.

Phosphorylation of CLN5 may also have some effect on the integrity of TJs of the BBB. Haorah et al. (15) reported that CLN5 phosphorylation could lead to BBB impairment. Furthermore, tyrosine phosphatase inhibition could induce loss of BBB integrity (24). In our research, phosphorylated CLN5 was detected in most HBs, including both cystic and solid HBs, but not in control brain. These results suggest that phosphorylation of CLN5 could also lead to the disturbances of BBB integrity in HBs. This could explain, in part, the mechanism of absence of TJs in some solid HBs that showed a high expression level of CLN5 mRNA and positive expression of CLN5 on microvessels in our immunohistochemical study.

The exact mechanism for dysregulation of CLN5 in ECs of HBs is still unknown. Considering the rich capillary network in HBs, we suspect that some angiogenic factors may play an important role in the absence of TJs in microvessels of HBs. It is well known now that VEGF could induce disruption of TJs in a protein kinase C-α-dependent manner (31). In HBs, there is a significant overexpression of VEGF in comparison with control brain. Fischer et al. (9) reported that hypoxia-induced changes of some TJ proteins in BBB damage are mediated by